OPEN

Thermally Induced Shape Modification of Free-standing Nanostructures for Advanced Functionalities

Ajuan Cui[1], Wuxia Li[1], Tiehan H. Shen[2], Yuan Yao[1], J. C. Fenton[3], Yong Peng[4], Zhe Liu[1], Junwei Zhang[4] & Changzhi Gu[1]

[1]Beijing National Laboratory of Condensed Matter Physics, Institute of Physics, Chinese Academy of Sciences, Beijing, 100190, China, [2]Joule Physics Laboratory, University of Salford, Manchester, M5 4WT, UK, [3]London Centre for Nanotechnology, University College London, London, WC1E 7JE, UK, [4]The Key Laboratory of Magnetism and Magnetic Materials of Ministry of Education, Lanzhou University, Lanzhou 730000, P. R. China.

Shape manipulation of nanowires is highly desirable in the construction of nanostructures, in producing free-standing interconnect bridges and as a building block of more complex functional structures. By introducing asymmetry in growth parameters, which may result in compositional or microstructural non-uniformity in the nanowires, thermal annealing can be used to induce shape modification of free-standing nanowires. We demonstrate that such manipulation is readily achieved using vertically grown Pt-Ga-C composite nanowires fabricated by focused-ion-beam induced chemical vapor deposition. Even and controllable bending of the nanowires has been observed after a rapid thermal annealing in a N_2 atmosphere. The mechanisms of the shape modification have been examined. This approach has been used to form electrical contacts to freestanding nano-objects as well as nano-'cages' for the purpose of securing ZnO tubs. These results suggest that thermally induced bending of nanowires may have potential applications in constructing three-dimensional nanodevices or complex structures for the immobilization of particles and large molecules.

T hree-dimensional (3D) micro/nanostructures and nanodevices have attracted significant interest in recent years. Various devices based on freestanding micro/nanostructures have shown excellent functionalities that planar nanodevices cannot achieve[1–6]. Since the fabrication techniques of nanowires and nanosheets are now relatively mature, an important focus has become the exploration of strategies for bending or folding nanowires and nanosheets to form more complex structures[7]. Shape modification of nanowires/sheets can be realized through several mechanisms, including thin-film stress[8], surface tension[9], inflating and deflating balloon joints[10], swelling of electro-active polymers[11] and magnetic interaction[12]. The size of the structures fabricated using some of the methods, such as swelling of electro-active polymers and magnetic interaction, have yet to reach length scales smaller than the order of a micron[13]. For thin-film-stress- and surface-tension-related methods, specific processes are required to bend the object and the procedure at present appears to be relatively complicated.

Focused-ion-beam (FIB)-induced chemical vapor deposition (CVD) and FIB-irradiation-induced bending[14–16] have been employed in the past to produce 3D conducting micro/nano-structures that can be used as free-standing electrodes[17]. These are not without their limitations: for instance, unwanted deposition near the structure, as a result of secondary electron and ion generation in the case of FIB-induced deposition, is usually difficult to avoid. Using ion-beam-irradiation-induced bending, arrays of freestanding nanocontacts can be prepared in parallel in the same processing step with reasonably good controllability and repeatability. However, upon irradiation with energetic ions, the properties of the original structures are generally affected[18]. Therefore, to construct nanodevices with advanced functionalities, a technique to produce freestanding and electrically connected nanostructures at a designated position that is free from the aforementioned side effects is highly desirable.

In this work, we examine thermally induced shape modification (TSM) of platinum-composite nanowires. This technique appears to satisfy the criteria above for the fabrication of freestanding site-specific nanoscale structures. In the paper we illustrate the technique for fabrication of freestanding Pt-Pt and Pt-Si nanocontacts with reliable electrical connections and for the construction of 'nano-cages' for securing crystalline particles. Our results demonstrate that TSM of Pt-composite nanowires can be employed effectively for the formation of

nanocontacts on freestanding objects. This is likely to be an important step towards the construction of 3D nanodevices with potential advanced functionalities, as well as for the immobilization of micro-/nano-objects for potential biological, magnetic and optical applications[19–22].
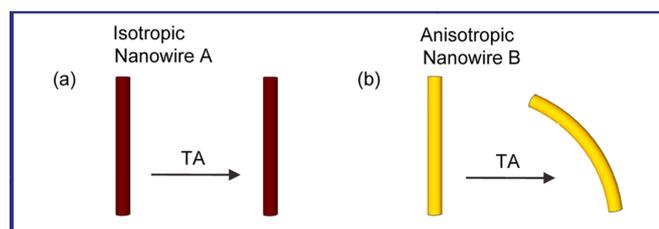
Results

Background and basic principles. Possible bending behaviors of free-standing nanowires upon thermal annealing are schematically shown in Figure 1. Uniform heating of an evenly stressed or a stress-free homogeneous freestanding wire leads to stress relaxation and microstructure changes which are uniform in different parts of the wire; thus, such an object undergoes no bending of the wire, as shown in Figure 1a. However, if there is some predefined profile of variation across the object in the stress, chemical composition or microstructure, then upon thermal annealing the object under examination may undergo a bending process, as shown in Figure 1b, owing to the relaxation of internal stress or because of non-uniform recrystallization. This implies that, by controlling and changing the compositional/structural profile of the material in the object, thermal annealing could be used to generate a designated degree of bending and so be used to form complex shapes or structures.
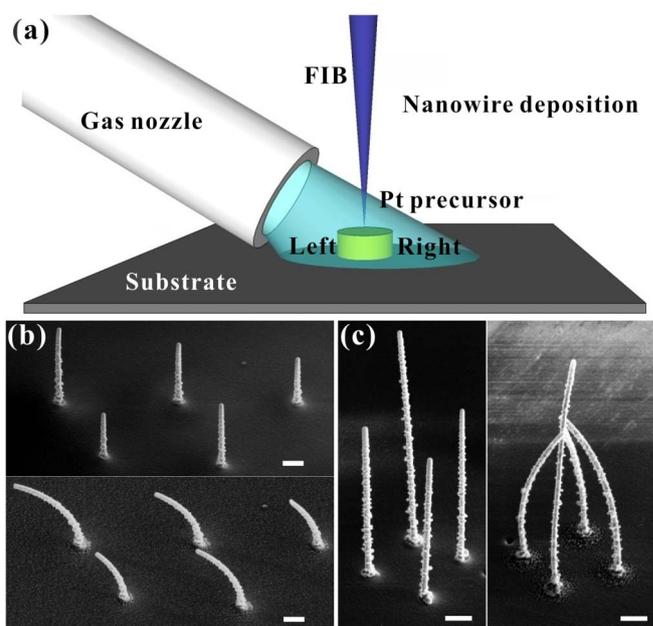
We now consider how such a profile variation across a nano-object grown by FIB-induced CVD might be achieved. Nano-objects grown by FIB-induced CVD are characterized by their shape and size, chemical composition and microstructure. The growth parameters may affect all of these features and thus will also be important in determining how a nano-object bends when it is thermally annealed. Key parameters are the precursor nozzle position, the ion beam current density, the ion beam scanning procedure, the growth temperature, the supporting substrate and the types of the gas precursor used. According to previous work relating to the dynamics of the growth mechanism[26], the deposition rate is mainly limited by two factors and can be divided into two regimes, namely, (i) a current-limited regime, within which the growth rate is independent of the gas flux; and (ii) a gas-flux-limited regime, within which the growth rate is independent of the current density. (In the experiments we describe later, although the ion beam current used for Pt nanowire growth was only 1 pA, the ion beam scanning area was also very small, about 7 nm in diameter (the size of a focused beam spot), corresponding to a current density of about 1.6×10^{19} charge s^{-1} cm^{-2}. Therefore, in our case the growth process was mainly determined by the diffusion of the gas molecules.) It has been shown experimentally that during FIB-induced CVD, the deposition yield is linearly proportional to the number of surface atoms excited by the collision cascades[23] and in both regimes the growth rate increases linearly with the dwell time, the time duration that the scanning beam stays at a particular location. Thus, in principle, the intrinsic properties of the as-deposited materials may be controlled by adjusting these parameters. In other words, they can be used to influence the chemical composition, and the microstructure along the axis or diameter of the grown features. In a system with rotational symmetry, the FIB deposition rate and composition would also have rotational symmetry. However, when the precursor gas molecules are provided by utilizing a single gas injection nozzle with the beam scanned on one side of the gas injection nozzle, the gas flux is not rotationally symmetric about the centre of the ion beam. Such a system can therefore lead to compositional/structural non-uniformity along the diameter while maintaining homogeneity along the wire length direction. Thus, by a judicious choice of the relative position of injection gas nozzle to the ion beam scan position during FIB growth, a desired inhomogeneity profile across the wires might be achievable. Below we show results of an experimental investigation into the prospect of such control.

Experimental design. We have used a model system to investigate the thermally induced shape modification processes. A gas-injection system installed in a FIB facility was used to grow vertical freestanding Pt-composite nanowires site-specifically in a single step. The gas-injection system used has a nozzle on one side of the growth area and this lack of rotational symmetry provides an opportunity to introduce non-uniformity across the cross section of the object deposited. Figure 2a is a schematic diagram of the experimental setup, showing the position of the gas injection system (the precursor nozzle) relative to the as-deposited nano-wire. Gases were delivered to the sample surface via a needle in close proximity to the surface ($\sim$50–150 µm) through the precursor nozzle. The FIB-induced CVD process involves three steps, namely the adsorption of gas molecules on substrate, dissociation/decomposition of gas molecules by the ion beam and deposition of the material, as well as removal of the organic ligands. Each step is controlled by different growth parameters[23]. The single precursor nozzle used for Pt nanowire deposition in our experiment provides reproducible gradients in composition, stress and defect density across the diameter of the as-deposited Pt nanowires.

Figure 2 | (a) A schematic diagram of the relative positions of the as-deposited nanowire and the precursor nozzle; (b) typical SEM images of an as-deposited vertically FIB-grown Pt nanowire array (upper image) and the same nanowires following annealing (lower image); (c) directional growth (by rotating the sample stage by 90° after each nanowire was grown) and bending of a group of four Pt nanowires (as-deposited in the image on the left and annealed on the right). The annealing was carried out in N$_2$ at 900°C for 60 s and the scale bars represent 1 µm.

Figure 1 | **An illustration of the bending mechnism of freestanding nanoobjects upon thermal annealing (TA).** (a) isotropic nanowires undergo no bending; (b) nanowires with anisotriopic cross-sections bend when annealed.

Thermally induced shape modification (TSM) of the nanowires. In order to investigate the effect of annealing on the morphology of nanowires grown as described above, a group of vertical Pt-composite nanowires of the same diameter (243 nm) but different heights (5.07 μm, 4.14 μm, 3.88 μm, 3.09 μm, and 2.95 μm) were grown (Figure 2). Figure 2b shows the SEM images taken at room temperature of Pt nanowires , as deposited (top image), and after rapid thermal annealing (RTA) in N_2 at 900°C for 60 s (bottom image). It can be seen that, although these nanowires were of different lengths, they all bent towards one particular direction, namely towards the precursor nozzle, which can also be observed from the image on the right hand side of Figure 2c, showing the TSM of the four Pt nanowires grown by rotating the stage 90° in turn. This illustrates that the desired bending of free-standing FIB-grown Pt composite nanowires can be achieved by the relative positioning of the precursor nozzle.

The effect of RTA was investigated in more detail. Firstly, a series of Pt nanowires with different lengths but the same diameter were deposited and underwent a nominally identical thermal annealing process. Figure 3a shows color-coded SEM images, with a viewing angle of 90° of the bent Pt-composite nanowires, which are 283 nm in diameter and 4.56 μm, 5.46 μm, 6.81 μm, 7.84 μm, 8.36 μm, 9.64 μm in length; the dimensions of the wires were measured after 5 RTA treatments, from 200°C to 600°C at intervals of 100°C for 1 min at each temperature. Figure 3b shows that the images of all the shape-modified wires may be superimposed on top of one another. These results indicate that all the wires bent in approximately circular arcs with a single radius of curvature. When the same experiment was repeated using wires grown on a tantalum (Ta) substrate, similar behavior was observed; this is shown in Figure 3c and 3d.

Quantitative analysis of the thermally induced shape modification. Since the bent nanowires observed were approximately circular arcs, the bending may be usefully parametrized by the radius of curvature, R, of the arc (Figure 3e). Through this parametrization, the influence of the annealing temperature on the thermally induced shape modification process was studied systematically. Pt composite nanowires were annealed sequentially using RTA at various annealing temperatures T_A, and observed (at room temperature) in the SEM after each annealing cycle. Each individual annealing cycle lasted for 60 s in a purged N_2 atmosphere, with a N_2 gas flow rate of 10 standard liters per minute (slpm); the temperature of successive anneals was increased from 200°C to 800°C in steps of 100°C. As for the results presented earlier, the nanowires were again observed to bend into approximately circular arcs. Figure 4a is a plot of $1/R$ as a function of T_A for a nanowire with length of 9.64 μm annealed at sequentially increasing values of T_A. In the lower temperature region, there was little thermally induced shape modification, but with increasing T_A, the nanowire bent more significantly, with a corresponding decrease in radius of curvature and therefore increase in $1/R$.

Figure 4b shows the TSM of Pt composite nanowires that underwent several annealing cycles at the same T_A. Substantial bending of the nanowires occurred during the initial annealing cycle, with smaller amounts of additional bending, and finally a saturation of bending, in subsequent annealing cycles. Figure 4c shows $1/R$ of a nanowire of 320 nm diameter and 7.36 μm length as a function of annealing cycle (N_{AC}) initially at $T_A = 500$°C, $N_{AC} = 1$–5, then $T_A = 600$°C, $N_{AC} = 6$–8, and finally $T_A = 700$°C, $N_{AC} = 9$. We discuss these results later.

As an alternative to rapid thermal annealing, *in situ* annealing was also conducted in a TEM through the heating to the substrate. The bending process was observed to be initiated from the base of the wire connected to the substrate, propagating to the tip of the wire in about 70 seconds until the shape modification was fully stabilized. We also consider the significance of this result later.
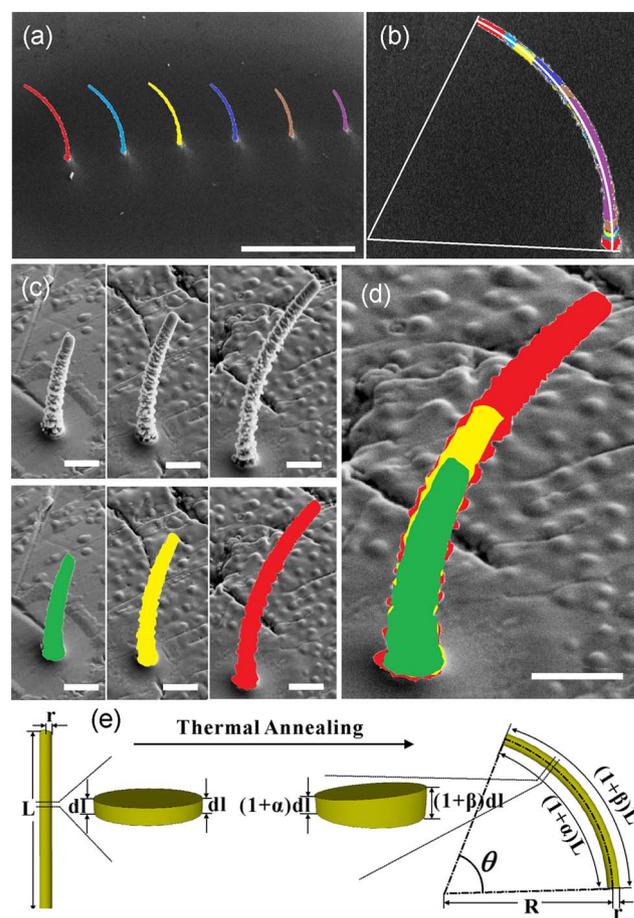
Figure 3 | (a) SEM image of a group of nanowires grown on a Si substrate, after 5 RTA treatments from 200°C to 600°C at intervals of 100°C for 1 min at each temperature; color-codes have been added to distinguish wires with different lengths; the scale bar in the micrographs is 10 μm; (b) A superposition of the images of the wires from (a), showing good alignment to a common arc of a circle; (c) SEM image of nanowires grown on a Ta substrate, after 5 RTA treatments at 500°C for 60 s. Color-coding has been introduced; (d) superposition of the wires from (c), showing good alignment to a common arc of a circle; the scale bar in micrographs (c) and (d) is 1 μm; and (e) an illustration depicting the simple model described in the text for bending of a nanowire following thermal annealing: wire length L, wire radius r and radius of curvature R, bending angle θ and expansion coefficients $\beta \geq \alpha$.

Model. Our experimental observations of wires bending in a circular arc, such as those shown in Figs. 3 and 4, demonstrate that the bending of the wires along their length is approximately uniform. The bending can be related to the difference between the inflation (the increase in volume of a part of the wire on annealing) of the two sides of the wire, using a simple model in which inflation of the nanowire on thermal annealing varies across its diameter but does not vary along the length of the nanowire. Consider a nanowire of length L as a large number of thin circular disks, of radius r and thickness dL, piled up along the long axis (see Figure 3e). If the bending of the wire is uniform along its length, each successive slice will add equally to the bend and therefore a circular arc will result. Denoting the inflation coefficients of the left and right side of the slice as α and β respectively, after annealing, the thickness of each slice becomes, $(1 + \alpha)dL$ on the left side and $(1 + \beta)dL$ on the right side; the total arc lengths of the left side and right side are, by simple integration, respectively $(1 + \alpha)L = (R - r)\theta$, $(1 + \beta)L = (R + r)\theta$, where θ is the angle subtended by the arc to the centre of the circle,
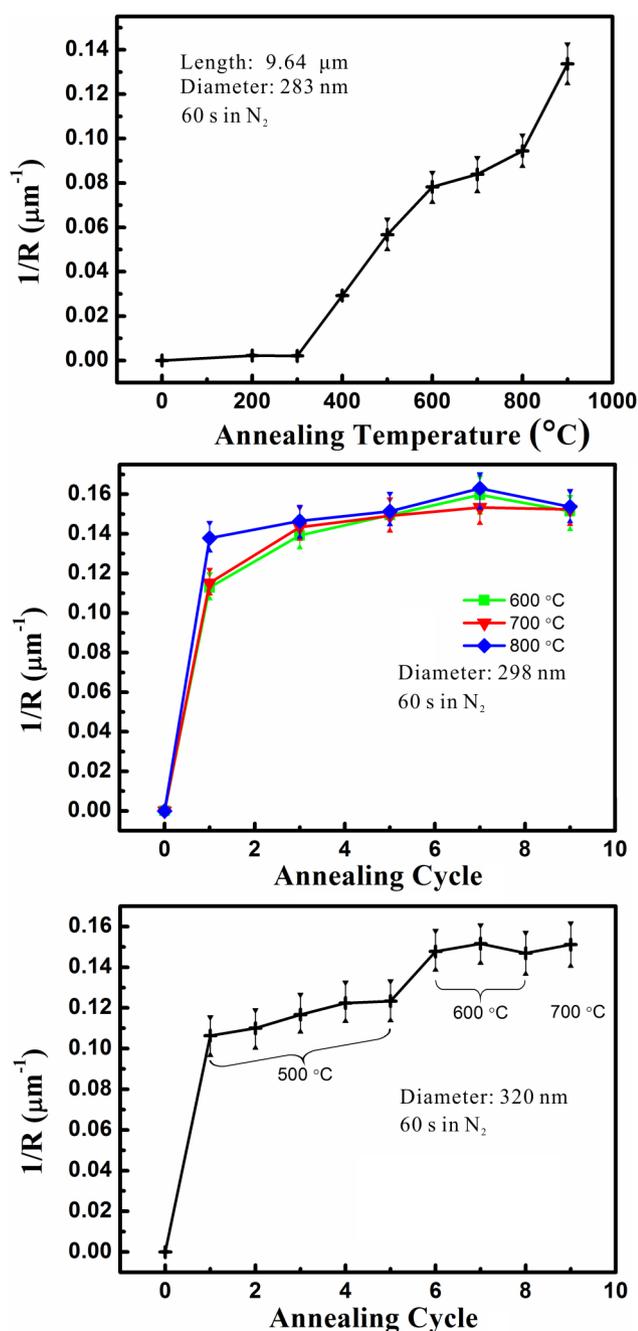
Figure 4 | The temperature-dependence of the bending process. (a) the inverse radius of curvature ($1/R$) as a function of T_A for a FIB-induced-CVD-grown Pt composite nanowire annealed by repeated RTA in N_2. The RTA duration was 60 s for each annealing cycle; (b) $1/R$ as a function of the number of RTA cycles (N_{AC}) for different fixed values of T_A for wires of nominally identical diameter and length; (c) $1/R$ for a nanowire of 320 nm width as a function of N_{AC} initially at $T_A = 500°C$, $N_{AC} = 1$–5, then $T_A = 600°C$, $N_{AC} = 6$–8, and finally $T_A = 700°C$, $N_{AC} = 9$. Extraction of R values was carried out by least-squares fitting of a circular arc to the nanowire in each image.

implying also $(\beta - \alpha) = 2r\theta/L$ and, since $\theta/L \approx 1/R$, $(\beta - \alpha) \approx 2r/R$. Using these equations, in principle the inflation coefficents α and β may be extracted by observation of the bent nanowires. In practice, the small sizes of α and β ($\alpha,\beta \ll 1$) and the uncertainties in determinations of r make an accurate determination of β or α difficult; however, the difference $(\beta - \alpha)$ may be determined directly by multiplying the wire diameter by $1/R$ (see e.g. Fig. 4).

Table one lists the size parameters of nanowires, RTA parameters, their corresponding radius of curvature, and the TSM in terms of R and the inflation coefficients. In the Discussion section, we explore how these changes are related to microstructure variations which we report in the next section.

Structural and compositional analysis. Similar Pt-composite nanowires were deposited on Si membranes for transmission electron microscopy (TEM). Electron energy loss spectroscopy (EELS) was used to examine the chemical composition of the wires across their diameter. FIB-deposited Pt-composite nanowires have previously been reported to have short-range order in microstructure with Pt nanocrystal grains buried in a carbon matrix[24]. Our preliminary results indicate qualitatively that the carbon content decreased with increasing distance from the gas injection nozzle. We assume that the variation in carbon content across the diameter is likely to exist because only a single gas injection nozzle was being used. The side of the wire closer to the precursor nozzle would have had more absorbed precursor gas molecules and experience less thorough decomposition of the precursor during the growth and hence contain more carbon. This process will be dependent on the type of precursors being used and the specific materials of the wires to be grown: Pt-composite nanowires have a sensitive dependence on the injector position but W nanowires show little dependence.

Discussion

Two observations in the structural and compositional analysis appear to explain the larger inflation of the far side of the wire during annealing:

(i) Qualitatively the carbon content was found to be higher on the side of the wires closer to the precursor nozzle whilst the Pt content was higher on the opposite side.

(ii) The TEM results indicate a size difference in the crystallographic domains, with the domains on the side closer to the gas injector being smaller. After annealing, the Pt particles were observed to increase in size and this increase was larger on the side further away from the gas injection nozzle.

These results suggest that the Pt nanowires we deposited using a single injection-gas nozzle were inhomogeneous in chemical composition and microstructure across the width of the wires and that the as-grown nanowires possibly possessed a distribution in the sizes of Pt nanoclusters. Previous time-resolved TEM measurements by Inkson and Dehm, during annealing at temperatures between 500°C and 650°C on FIB-deposited Pt-composite nanowires, showed that the thermal annealing process can result in particle coalescence and growth inside the wire on a timescale comparable to the observation in the present study[24]. This implies that, in our system also, non-uniform recrystallization through coalescence of neighboring crystalline clusters occurred upon annealing, at a rate which may be limited by an activation-energy-determined diffusion process, and resulted in the non-uniform volume change on the two sides and the associated bending of the wire, certainly between 580°C and 650°C, the range in which Inkson and Dehm observed microstructure changes, as suggested by the results show in in Figure 4c. Sheldon et al. reported that intrinsic tensile stresses could be created by the coalescence of neighboring islands during film growth by a variety of techniques[25]; this coalescence of neighboring nano-crystal grains may be a similar process to the Pt grain growth during annealing in this work, with intrinsic tensile stresses responsible for additional bending. Interestingly, Inkson and Dehm did not observe microstructure changes during repeated cycles to temperatures between 500°C and 550°C. This may suggest that the bending we observe at temperatures at and below 500°C (see Fig. 4a) may not be associated with grain growth or crystallization; instead it may be associated particularly with the *non-uniformity* of our nanowires,
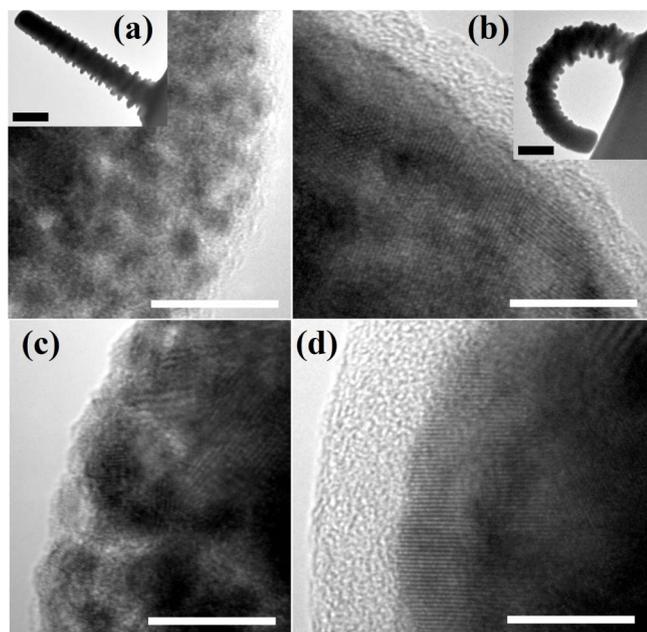
perhaps through a mechanism of internal stress relaxation at temperatures below 550°C.

The wires have a morphology which is somewhat 'spiky', as if they were made of slightly irregularly shaped plates stacked along the wire length. This may be playing some role: in a real-time TEM observation during an *in situ* annealing, the outer edge of the wire projection appeared to have become smoother, suggesting that the 'spikes' were 'providing' materials in the thermally induced shape modification process. This can also be observed by comparing the images in the inset of Figure 5a and 5b.

The relatively short time for the completion of the TSM process as observed in the *in situ* TEM annealing experiment implies that the re-crystallization process may happen over a relatively narrow temperature interval with the progression of the bending from the wire base highlighting the passage of a particular isotherm up through the wire as it heats. Previous TEM measurements on Pt-composite nanowires have identified 580–650°C as a threshold for crystallization[24], which supports the conclusion that bending in our nanowires is primarily driven by recrystallization, as well as being consistent with the change in smaller radius of curvature achieved through annealing at temperatures of 600°C or above.

For the results shown in Fig. 4 as well as in Table 1, both the RTA temperature and the number of cycles influence the cluster growth and hence the wire bending process. The saturation of the bending angle of nanowires is likely to indicate termination of cluster growth. Inkson and Dehm observed nucleation of crystallites on timescales below 1 s, with growth of the particles continuing to at least 30 s; this suggests that the microstructure may well be continuing to evolve at annealing times of a few minutes, consistent with our observations of apparent small increases of $1/R$ after anneal times in the order of minutes. From Table 1, it can be seen that the TSM parameters also depend qualitatively on the diameter of the nanowires. The $(\beta - \alpha)$ increases with an increase of the wire diameter, annealing temper-

Table 1 | TSM of Pt nanowires in terms of the inflation coefficients (see main text) for Pt nanowires of diameter D, length L and annealed at annealing temperature T_A with number of annealing cycles N_{AC}. θ_{off} is the angle by which the fit-circle diameter to the base of the nanowire deviates from the horizontal
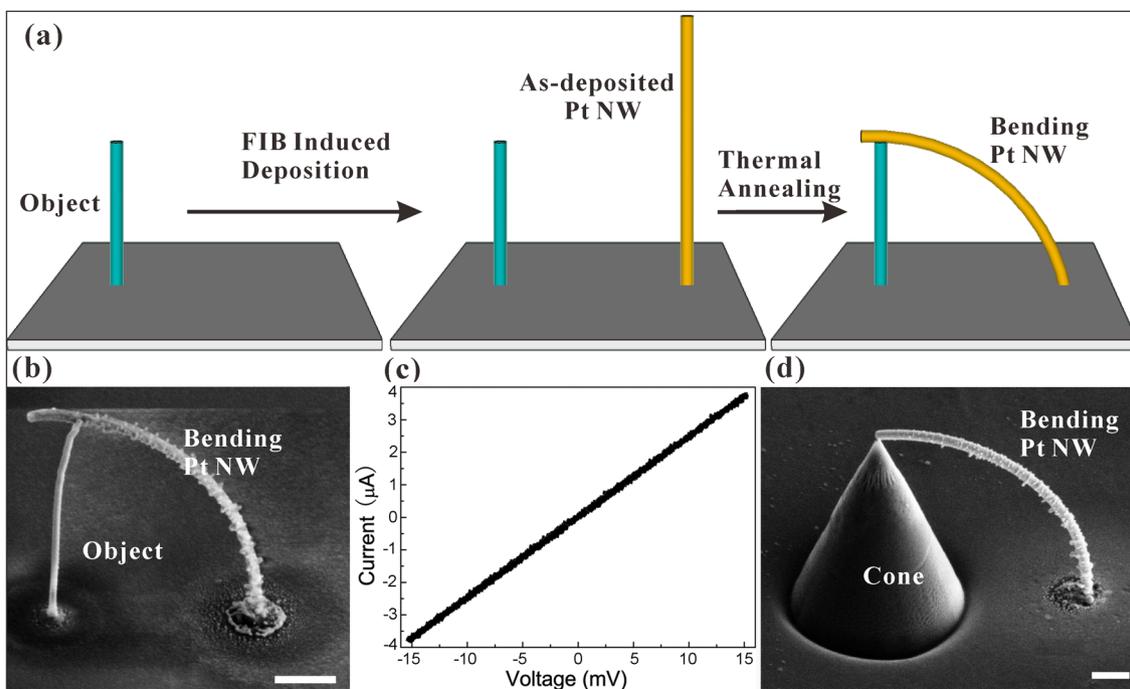
D(nm)	L(μm)	T_A(°C)	N_{AC}	R(μm)	$\beta - \alpha$	θ_{off}(deg.)
283	9.64	200	1	449.57	0	0.7
283	9.64	300	1	479.12	0	0.7
283	9.64	400	1	34.17	0.01	−2.4
283	9.64	500	1	17.66	0.02	1.7
283	9.64	600	1	12.78	0.02	1.5
283	9.64	700	1	11.92	0.02	2.5
283	9.64	800	1	10.59	0.03	4
283	9.64	900	1	7.48	0.04	9.6
298	7.03	600	1	8.86	0.03	1.4
298	7.03	600	9	6.61	0.04	1.5
298	7.42	700	1	8.68	0.03	0.8
298	7.42	700	9	6.56	0.05	0.1
298	7.81	800	1	7.26	0.04	−1.6
298	7.81	800	9	6.51	0.05	−1.8
344	6.06	800	1	3.20	0.11	0.6
344	6.06	800	3	3.07	0.11	2.2
344	6.06	800	5	3.20	0.11	−6.3

ature and the number of annealing cycles. These results are in good agreement with expectations.

Based on our simple model of the bending, it should be expected that the wire is vertical at its base so that the centre of the fitted circle should be at the same vertical level as the base of the nanowire in each image. θ_{off} in Table 1 shows the angle by which the fit-circle diameter to the base of the nanowire deviates from the horizontal. In most cases it is rather small, again indicating the applicability of the simple model to these results and showing that the nanowire does not have a significant non-uniform reaction with the substrate at its base.

Whilst these intriguing TSM characteristics of Pt-composite nanowires deserve further investigation, they have already opened up interesting possibilities for devices. We showed above (Fig. 2b) that, regardless of their length, nanowires bend towards a particular direction, namely towards the precursor nozzle. By rotating the sample stage, the position relative to the gas injection nozzle of each individual nanowire can be adjusted and this can also be exploited to grow Pt nanowires which bend in different directions during annealing and even meet at a point. For example, the left-hand image of Figure 2c shows a group of four Pt nanowires grown one by one, rotating the stage by 90° after the deposition of each wire so that, for any given wire of the four, the side of the wire closest to its pair diagonally opposite was the side nearest the precursor nozzle during its deposition. Upon annealing the wires, TSM occurs, as shown on the left-hand side of Fig. 2c, leading to the image on the right hand side of Figure 2c. This illustrates that a desired degree of bending of free-standing FIB-grown Pt-composite nanowires can be achieved by controlling the relative positioning of the precursor nozzle.

Electric contacts were constructed on freestanding tungsten composite nanowires. Figure 6a is a schematic diagram showing the process. Figure 6b is an SEM image of a typical freestanding Pt-W nanocontact. The bending direction was controlled by adjusting the relative positions of the Pt-composite nanowire to the precursor nozzle and the bending extend was chosen based on the height of the wire to be bent and its distance to the target. By a careful choice of growth parameters and annealing conductions, a solid contact or even a nanogap can be obtained. Figure 6c shows the room-temperature current-voltage (I–V) characteristics for a freestanding air-bridge W-Pt nanostructure, measured in a two-probe configuration. Linear I–V characteristics were observed with good reproducibility, indicating that the resulting freestanding electrode was robust and

Figure 5 | TEM images on the edge of the as-deposited and annealed platinum composite nanowires. (a) the inner edge of the as-deposited nanowire; (b) the inner edge of the annealed nanowire; (c) the outer edge of the as-deposited nanowire; (d) the outer edge of the annealed nanowire; the inset in (a) and (b) shows the TEM image of the as-deposited nanowire and that annealed in-situ in the TEM system, showing the same arc shape as observed in the rapid thermal annealing. The scale bar is 10 nm for all images. The scale bar in the inset of (a) and (b) is 1 μm. TEM images were taken at room temperature.

Figure 6 | (a) A schematic diagram showing the process of constructing a nanoelectrode on a freestanding functional entity by thermal-annealing-induced bending of FIB-grown Pt nanowires. The sequence shows: locating a freestanding target, the growth of a vertical nanowire in the vicinity of the target, and the construction of freestanding nanocontact through thermal annealing; (b) a typical SEM image of the formed W-Pt air-bridge structure; (c) the current-voltage curve of a W-Pt joint freestanding nanostructure, showing linear current-voltage characteristics; (d) a point-contact formed on the exact tip position of a Si cone. The scale bar represents 1 μm.

ohmic in nature. Following the approach previously reported[14], the contact resistance of the W-Pt junction and the resistivity of the annealed suspended Pt nanowire was estimated to be a few tens of ohms and a few thousands of micro ohms•cm, respectively. Si cones were also fabricated and the thermally induced shape modification method was used to bend FIB-grown Pt-composite nanowires to form a nanocontact on the tip of the cone, as shown Figure 6d, further demonstrating that this technique has very good controllability.

The immobilization of micro-/nano-objects has been intensely studied and has potential applications in bioscience[27] and quantum optics[28], and much interesting work has also been conducted with optical trapping[29]. Here we demonstrate the immobilization of micro-/nano-objects using freestanding cages formed with arc-shaped conductive nanowires. The cages were fabricated using Pt-composite nanowires through thermal annealing induced bending. Figure 7 shows SEM images of the fabrication process: the growth of vertical Pt-composite nanowires (Figure 7a and 7b) around the object followed by thermal annealing induced bending (Figure 7c and 7d). In this work, a double-decker ZnO crystalline 'tub' was encased. The cages are made of a number of freestanding nanowires with designated length and direction and degree of bending. The cage has a large free-surface area, controllable size and good electrical conductivity. Such cages could potentially be used for volume-selective entrapment of bio-sensitive, magnetic and optical beads, particles and macro molecules. In this approach, the encaged object can take a certain degree of motion when an external field is applied, and the particular object can be relocated and re-tested. It is also interesting to point out that the immobilized object is not fully enclosed, and this feature could be used for the investigation of *in situ* dynamic motion and reaction[30].

To summarize, freestanding 3D conductive structures were designed and fabricated through thermally induced shape modification based on FIB-deposited Pt-composite nanowires which were deliberately grown to realize inhomogeneous compositional/

structural distribution across the wire diameter. Such inhomogeneity was utilized for successful shape manipulation. The thermally induced shape modification was found to occur at temperatures ranging from 200°C up to 900°C. This shape manipulation could
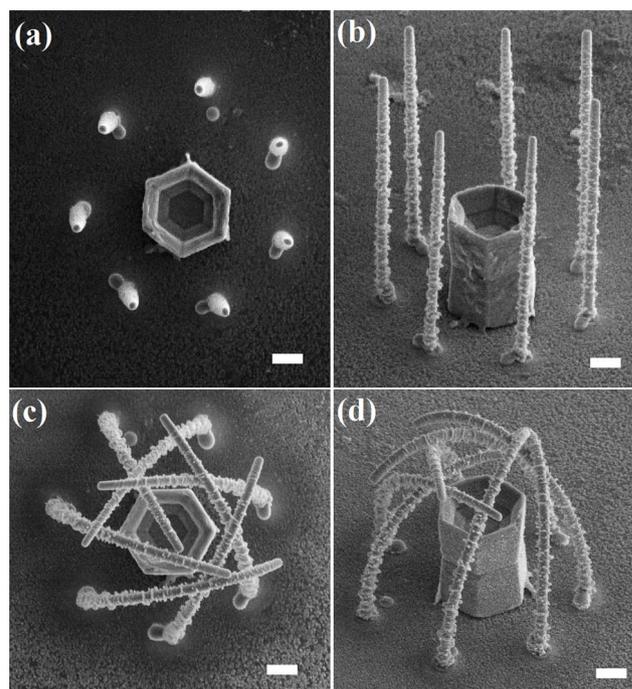
Figure 7 | The construction of a Pt wire nanocage for single crystalline ZnO tub imobilization. (a) the SEM top-view image and (b) side-view image of the nanocage structure prior to annealing; (c) top view image and (d) side-view image of the completed Pt nanocage after RTA, with the ZnO tub encapsulated inside the cage. The scale bar is 1 μm.

provide significant flexibility for efficient fabrication of out-of plane nanostructures based on various types of material systems. The resulting wires generally possess an arc shape and the bending angle of the nanowire can be precisely controlled by growth parameters, annealing temperature and annealing duration/cycle. Both the arc shape and the similar radius of curvature for the same type of nanowires with different lengths, when processed using nominally identical annealing processes, indicate that bending occurs uniformly along the length of the wires. A simple model has been developed to describe the behavior of the bending. Solid electrical contacts were constructed on freestanding W nanowires and Si cones using the technique; electrical characterizations confirmed a good and reliable electrical connection. Nano-cages have also been fabricated to physically confine micro-/nano crystalline ZnO tubs, and this method could potentially be used for particle immobilization. These results indicate that thermally induced shape modification of freestanding nanowires can be effectively employed to construct 3D structures and form reliable contacts with potential for advanced functionalities.

Methods

Growth of Pt-composite nanowires. Platinum (Pt) and tungsten (W) nanowires used in this study were grown on SiO_2/Si substrates by FIB induced chemical deposition with $(CH_3)_3Pt$ ($CpCH_3$) and $W(CO)_6$ respectively as precursors. The system used is a dual beam FIB/scanning electron microscope (SEM) (FEI DB 235). The ion column has a singly charged liquid gallium ion source, which is placed at an angle of $52°$ to the vertically oriented electron beam column. During growth, the precursor molecules were injected to the area through a gas injection nozzle, where the FIB was scanned by the scanning strategy of 'spot-mode' with ion beam current of 1 pA. The sample chamber pressure was about 10^{-5}–10^{-6} mbar during deposition.

The length of the nanowire was controlled by the deposition time, the diameter of the nanowire was determined by the focus level of the ion beam. By sample-stage rotation, the relative position of each wire to the gas nozzle can be precisely adjusted, through which the bending direction of the nanowire upon annealing was controlled.

Thermal annealing. In this work, thermal annealing treatments were conducted in a rapid thermal annealing (RTA) furnace purged with a constant flow of N_2 gas. The annealing duration and annealing temperatures were adjusted. *In situ* annealing took place in a TEM facility, in which a home-made sample stage was used. With an electrical current to a heating element, nanowires on the stage can be heated.

The structural and compositional properties analysis. High-resolution transmission electron microscopy (HRTEM) was used to study the microscopic structure of the wires, and electron energy-loss spectroscopy (EELS) was used to probe the chemical composition distribution of the wires.

The electrical property measurement. The contact properties and the resistivity of the constructed 3D Pt-Pt, W-Pt and Si-Pt nanostructures were measured in a two-terminal configuration using the Electrical Transport Option (ETO) module installed in a Quantum Design Physical Properties Measurement System (PPMS).

1. Valentine, J. *et al.* Three-dimensional optical metamaterial with a negative refractive index. *Nature* **455**, 376–379 (2008).
2. Gouma, P. *et al.* Nanosensor and breath analyzer for ammonia detection in exhaled human breath. *IEEE Sens. J.* **10**, 49–53 (2010).
3. Tian, B. *et al.* Three-dimensional, flexible nanoscale field-effect transistors as localized bioprobes. *Science* **329**, 830–834 (2010).
4. Noda, S., Tomoda, K., Yamamoto, N. & Chutinan, A. Full three-dimensional photonic bandgap crystals at near-infrared wavelengths. *Science* **289**, 604–606 (2000).
5. Romans, E. J. *et al.* Three-dimensional nanoscale superconducting quantum interference device pickup loops. *Appl. Phys. Lett.* **97**, 222506 (2010).
6. Morita, T. *et al.* Free-space-wiring fabrication in nano-space by focused-ion-beam chemical vapor deposition. *J. Vac. Sci. & Technol. B* **21**, 2737–2741 (2003).
7. Zhou, W. & Wang, Z. L. (Eds.). Three-dimensional nanoarchitectures: Designing next-generation devices. *Springer*, (2011).
8. Luo, J. K. *et al.* Modelling and fabrication of low operation temperature microcages with a polymer/metal/DLC trilayer structure. *Sensors Actuat. A-Phys.* **132**, 346–353 (2006).
9. Py, C. *et al.* Capillary origami: Spontaneous wrapping of a droplet with an elastic sheet. *Phys. Rev. Lett.* **98**, 156103 (2007).
10. Lu, Y.-W. & Kim, C.-J. Microhand for biological applications. *Appl. Phys. Lett.* **89**, 164101 (2006).
11. Jager, E. W. H., Inganäs, O. & Lundström, I. Microrobots for micrometer-size objects in aqueous media: Potential tools for single-cell manipulation. *Science* **288**, 2335–2338 (2000).
12. Iwase, E. & Shimoyama, I. Multistep sequential batch assembly of three-dimensional ferromagnetic microstructures with elastic hinges. *J. Microelectromech. S.* **14**, 1265–1271 (2005).
13. Leong, T. G., Zarafshar, A. M. & Gracias, D. H. Three-dimensional fabrication at small size scales. *Small* **6**, 792–806 (2010).
14. Li, W. & Warburton, P. A. Low-current focused-ion-beam induced deposition of three-dimensional tungsten nanoscale conductors. *Nanotechnology* **18**, 485305 (2007).
15. Borschel, C. *et al.* Permanent bending and alignment of ZnO nanowires. *Nanotechnology* **22**, 185307 (2011).
16. Arora, W. J. *et al.* Membrane folding by helium ion implantation for three-dimensional device fabrication. *J. Vac. Sci. Technol. B* **25**, 2184 (2007).
17. Cui, A. *et al.* Freestanding nanostructures for three-dimensional superconducting nanodevices. *Appl. Phys. Lett.* **100**, 143106 (2012).
18. Štrbík, V. *et al.* Effect of galliun focused ion beam irradiation on properties of $YBa_2Cu_3O_x/La_{0.67}Sr_{0.33}MnO_3$ heterostructures. *J. Electr. Eng.* **62**, 109 (2011).
19. Yang, A. H. J. *et al.* Optical manipulation of nanoparticles and biomolecules in sub-wavelength slot waveguides. *Nature* **457**, 71–75 (2009).
20. Grigorenko, A. N. *et al.* Nanometric optical tweezers based on nanostructured substrates. *Nat. Photon.* **2**, 365–370 (2008).
21. Rahmani, A. & Chaumet, P. C. Optical trapping near a photonic crystal. *Opt. Express* **14**, 6353–6358 (2006).
22. Mandal, S., Serey, X. & Erickson, D. Nanomanipulation Using Silicon Photonic Crystal Resonators. *Nano Lett.* **10**, 99–104 (2009).
23. Utke, I., Hoffmann, P. & Melngailis, J. Gas-assisted focused electron beam and ion beam processing and fabrication. *J. Vac. Sci. & Technol. B* **26**, 1197–1276 (2008).
24. Inkson, B. J. & Dehm, G. Thermal stability of Pt nanowires manufactured by Ga+ focused ion beam (FIB). *MRS Proceedings* **777**, (2003).
25. Sheldon, B. W., Lau, K. H. A. & Rajamani, A. Intrinsic stress, island coalescence, and surface roughness during the growth of polycrystalline films. *J. Appl. Phys.* **90**, 5097–5103 (2001).
26. Utke, I. Nanofabrication using focused ion and eectron beams: Principles and applications. *Oxford University Press*, (2012).
27. Hegner, M. *et al.* Modified DNA immobilized on bioreactive self-assembled monolayer on gold for dynamic force microscopy imaging in aqueous buffer solution. *J. Vac. Sci. Technol. B* **14**, 1418 (1996).
28. Gaur, G., Koktysh, D. S. & Weiss, S. M. Immobilization of quantum dots in nanostructured porous silicon films: Characterizations and signal amplification for dual-mode optical biosensing. *Adv. Funct. Mater.* (2013).
29. Neuman, K. C. & Block, S. M. Optical trapping. *Rev. Sci. Instrum.* **75**, 2787–2809 (2004).
30. Bopp, M. A. *et al.* The dynamics of structural deformations of immobilized single light-harvesting complexes. *P. Natl. Acad. Sci.* **96**, 11271–11276 (1999).

Author contributions

W.L., A.J.C., C.Z.G. and T.H.S. conceived and designed the experimental and theoretical work. A.J.C. performed the FIB and RTA experiments, Y.Y., Y.P. and J.W.Z. conducted the TEM experiments and contributed to the bending mechanism discussion, Z.L. carried out the electrical measurements. Image data-analysis was carried out by J.C.F. and A.C. W.L., A.J.C. and J.C.F. drafted the manuscript which has been further revised by all authors.

Additional information

Competing financial interests: The authors declare no competing financial interests.

How to cite this article: Cui, A. *et al.* Thermally Induced Shape Modification of Free-standing Nanostructures for Advanced Functionalities. *Sci. Rep.* **3**, 2429; DOI:10.1038/srep02429 (2013).